Human Molecular Genetics, 2009, Vol. 18, No. 2 **289–303**
doi:10.1093/hmg/ddn356
Advance Access published on October 29, 2008

Convergent extension movements and ciliary function are mediated by *ofd1*, a zebrafish orthologue of the human oral-facial-digital type 1 syndrome gene

Maria I. Ferrante[1,†], Leila Romio[2,3,†], Silvia Castro[3], John E. Collins[1], David A. Goulding[1], Derek L. Stemple[1,*], Adrian S. Woolf[2] and Stephen W. Wilson[3]

[1]Wellcome Trust Sanger Institute, Wellcome Trust Genome Campus, Cambridge CB10 1SA, UK, [2]Nephro-Urology Unit, UCL Institute of Child Health, London WC1N 1EH, UK and [3]Department of Cell and Developmental Biology, UCL, London WC1E 6BT, UK

Received July 22, 2008; Revised and Accepted October 26, 2008

In humans, *OFD1* is mutated in oral-facial-digital type I syndrome leading to prenatal death in hemizygous males and dysmorphic faces and brain malformations, with polycystic kidneys presenting later in life in heterozygous females. To elucidate the function of Ofd1, we have studied its function during zebrafish embryonic development. In wild-type embryos, *ofd1* mRNA is widely expressed and Ofd1-green fluorescent protein (GFP) fusion localizes to the centrosome/basal body. Disrupting Ofd1 using antisense morpholinos (MOs) led to bent body axes, hydrocephalus and oedema. Laterality was randomized in the brain, heart and viscera, likely a consequence of shorter cilia with disrupted axonemes and perturbed intravesicular fluid flow in Kupffer's vesicle. Embryos injected with *ofd1* MOs also displayed convergent extension (CE) defects, which were enhanced by loss of Slb/Wnt11 or Tri/Vangl2, two proteins functioning in a non-canonical Wnt/Planar Cell Polarity (PCP) pathway. Pronephric glomerular midline fusion was compromised in *vangl2* and *ofd1* loss of function embryos and we suggest this anomaly may be a novel CE defect. Thus, Ofd1 is required for ciliary motility and function in zebrafish, supporting data showing that Ofd1 is essential for primary cilia function in mice. In addition, our data show that Ofd1 is important for CE during gastrulation, consistent with data linking primary cilia and non-canonical Wnt/PCP signalling.

INTRODUCTION

Oral-facial-digital syndrome type 1 (OFD1) syndrome occurs in 1:50-250,000 live births (1,2). Hemizygous XY males usually undergo poorly explained prenatal death, whereas heterozygous XX females are born with facial dysmorphology, digital abnormalities and midline clefts. OFD1 syndrome sometimes features polycystic kidneys, with each cyst comprising a cluster of glomerular podocyte epithelia protruding into a dilated Bowman's space (3,4), and the Dandy-Walker anomaly, comprising dilated fourth ventricle and hydrocephalus (5). OFD1 is expressed prenatally in organs affected by the syndrome (6), with protein detected in centrosomes and the basal bodies of primary cilia (7). OFD1 has also been detected in Cos-7 cell nuclei (8). *OFD1* mutations usually lead to truncations (9,10), thus generating non-functional products. Human *OFD1* escapes X-inactivation (11) and heterozygous XX cells, therefore, probably contain a diminished amount of OFD1, while hemizygous XY cells have no functional protein.

Mutations of ciliary proteins cause several human diseases and also produce mouse and zebrafish phenotypes (12–14). By generating leftward flow in the mouse embryonic node

*To whom correspondence should be addressed. Tel: +44 1223496857; Fax: +44 1223494919; Email: ds4@sanger.ac.uk
†The authors wish it to be known that, in their opinion, the first two authors should be regarded as joint First Authors.

and zebrafish Kupffer's vesicle (KV), active motile cilia establish organ laterality (15,16), and they also mediate cerebrospinal fluid movement and respiratory tract mucous clearance. Primary cilia are generally not actively motile but transduce signals into cells. Located on mammalian renal epithelia they sense renal tubular flow by bending, thus instigating intracellular signalling which maintains epithelial differentiation (12,17–19). Mammalian primary cilia contain Sonic hedgehog (Shh) pathway components (20,21) and disruption of intraflagellar transport, and hence cilia formation, perturbs Shh signalling (22).

Ofd1 null XY mice have embryonic nodes lacking cilia, explaining left-right axis specification defects (23). Their ventral neural tubes are abnormally-specified with Shh target genes downregulated (23). Because murine *Ofd1* is X-inactivated (11), *+/Ofd1* XX mice are mosaics of cells replete with, and devoid of, Ofd1. They are born with glomerular cysts lacking primary cilia, and have polydactyly with aberrant anterior gene expression in limb buds (23).

Ciliary defects affect Wnt signalling (17,24,25) and, conversely, Wnt pathway proteins facilitate cilia formation (26,27). Cilia may mediate a switch from canonical β-catenin Wnt signalling to non-canonical Planar Cell Polarity (PCP) signalling (17). PCP signalling regulates convergent extension (CE) movements (28–30), during which cells from lateral regions converge towards the midline and intercalate, facilitating embryonic narrowing and antero-posterior axis extension (31). Disruption of Bardet-Biedl syndrome (BBS) ciliary proteins accentuates the CE defects seen upon disruption of the PCP pathway genes *tri/vangl2* or *slb/wnt11* (30,32–34). Nothing is known, however, about the possible relationship between Ofd1 and CE.

Here, we have studied Ofd1 in developing zebrafish (*Danio rerio*) embryos. Zebrafish *ofd1* has been identified (11) and the gene encodes a protein with a LisH domain and coiled-coil domains homologous to human OFD1. We have disrupted Ofd1 by injection of antisense morpholinos (MOs) and found that injected embryos display a typical ciliary phenotype with bent body, laterality defects and oedema. We found that cilia in the KV are shorter than normal and the flow inside this structure appears to be altered. We also found that Ofd1 has a role in CE and we assessed potential genetic interactions of *ofd1* with *wnt11* and *vangl2* using MOs and *trilobite* (*vangl2)* mutants (33). Collectively, the results show that Ofd1 is required for normal ciliary motility and function in zebrafish, supporting recent data that the Ofd1 gene affects the biology of primary cilia in mice (23), and the contention that human OFD1 syndrome is indeed a ciliopathy (35). They also show that Ofd1 plays a role in convergent-extension during normal gastrulation, consistent with recent data showing links between ciliary signal transduction and non-canonical Wnt signalling (24,36).

RESULTS

ofd1 is widely expressed and Ofd1-GFP localizes to centrosomes/basal bodies

Reverse transcriptase–polymerase chain reaction (RT–PCR) and *in situ* hybridization (ISH) showed that *ofd1* is widely expressed in embryos from one-cell stage through 5 days post-fertilization (Fig. 1A–H and data not shown). At the eight-somite stage, *ofd1* is expressed in KV (Fig. 1C and D). From 24 h post fertilization (hpf), *ofd1* expression is accentuated in lateral line primordia, otic vesicles and neuromasts, which contain ciliated epithelia (Fig. 1E–H and Supplementary Material, Fig. S1).

To determine the sub-cellular localization of Ofd1, we injected a construct encoding a green fluorescent protein (GFP)-tagged version of the protein. Punctate fluorescence was observed in diverse structures including notochord, retinal and otic vesicle epithelia, and neural tube, in an overlapping distribution with γ-tubulin, consistent with basal body/centrosomal localization (Fig. 1I–T). Injected embryos appeared morphologically normal.

Disruption of Ofd1 produces curved bodies and a wide spectrum of malformations

To address the requirements for Ofd1 during development, we injected *ofd1* MOs into one-cell stage embryos, using either a translation blocking (ATG) or one of two splicing-perturbing (SPL6 and SPL7) MOs. Each produced a similar dysmorphic spectrum (Table 1 and data not shown). By 28 hpf, *ofd1* MO-injected embryos displayed upwards or downwards body axis curvatures (Fig. 2A and B), with aberrant curvature maintained over the following days (Fig. 2C–H and data not shown). Some 28 hpf embryos showed reversed cardiac jogging, while others had medially positioned hearts (not shown). The heart chambers were also abnormally shaped in a number of embryos and pericardial oedema occurred from 48 hpf, with systemic oedema by 96 hpf (Fig. 2C–H and data not shown). Hydrocephalus occurred between 24 and 48 hpf, sometimes with abnormal tissue bridges in the hindbrain ventricle (Fig. 2I–L). In some embryos, otoliths were more numerous and smaller than normal (Fig. 2M and N) and incomplete fusion of the choroid fissure of the eye (coloboma) was occasionally noted (Fig. 2O and P). By day 5, jaws were blunted with Meckel's cartilage containing rounded cells that were disorganized when compared to the normal columnar organization (Fig. 2Q and R). At equivalent concentrations, a five base-mismatched *ofd1* MO produced no such defects (not shown). To confirm translation-blockade by the *ofd1* ATG MO, we demonstrated that co-injecting it with *ofd1-GFP* mRNA downregulated the expected fluorescence pattern (Fig. 1K and L). Efficacies of *ofd1* SPL MOs were assessed by RT–PCR with primers spanning the targeted site; in both cases aberrant splice products were detected, although diminished normal cDNA remained (Supplementary Material, Fig. S2 and data not shown).

Pronephric fusion and filtration in *ofd1* MO-injected embryos

Filtering pronephric glomeruli form by 40 hpf, allowing elimination of ingested water (37). To test whether kidney function was disturbed following depletion of Ofd1, low molecular weight (10 kDa) FITC-dextran was injected into the pericardial space and followed over 20 h. We noted that injection of 10 kDa FITC-dextran into the interstitial space in front of

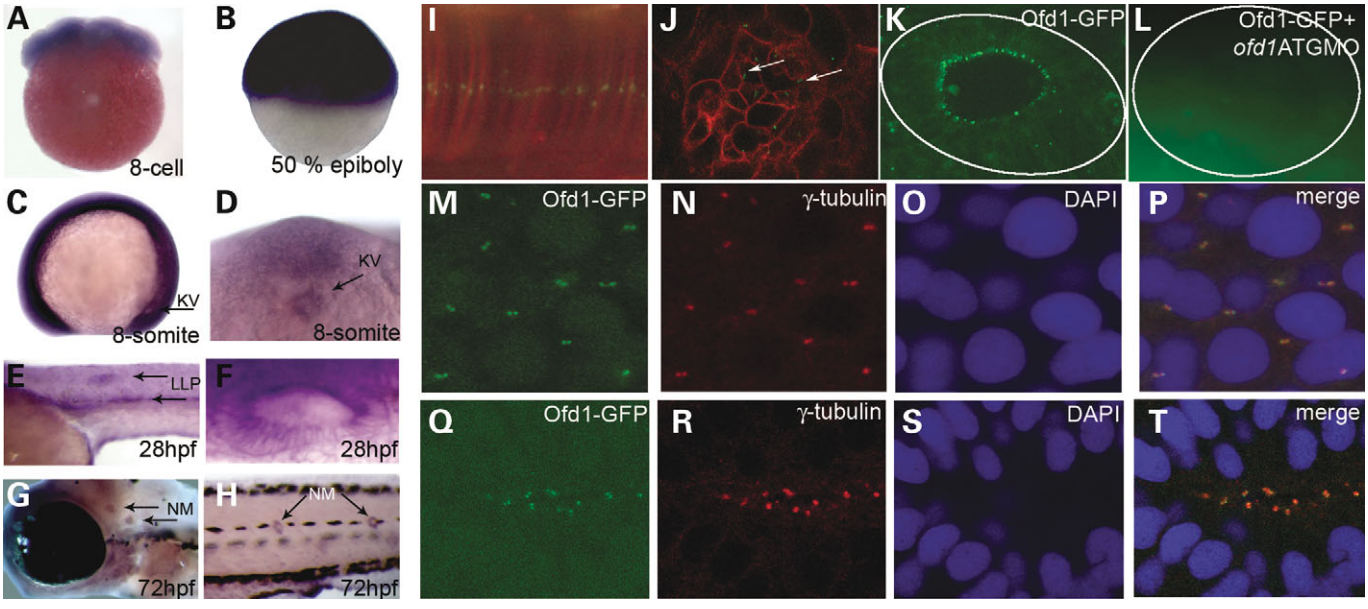

Figure 1. Expression of *ofd1* during zebrafish development and Ofd1-GFP localization to centrosomes and basal bodies. (**A**–**H**) Lateral views of embryos analysed by whole-mount ISH; anterior is to the left and dorsal is to the top, except in A, where the animal pole is uppermost, and in D, which is a ventral view. Positive *ofd1* signal is purple. (A) Eight cell stage embryo. (B) 50% epiboly (gastrula) embryo. (C) Eight-somite embryo, arrow points to the Kupffer's vesicle (KV). (D) Magnified view of the KV in the eight-somite embryo seen from the ventral aspect; note *ofd1* expression. (E) Detail of the body at 28 hpf, with signal evident in the lateral line primordia (LLP) (arrows). (F) Otic vesicle at 28 hpf. (G and H) Arrows indicate neuromasts (NM) in the head and trunk, respectively, at 72 hpf. (I) Confocal image showing a linear punctuate pattern of fusion protein (green) in the notochord of a 10-somite embryo (lateral view), representing centrosomes in the stack of flat cells. (J) A punctate, basal body-like pattern (arrows) on the apical surface of retinal epithelial cells in 24 hpf embryos. Cell membranes in (**I**) and (**J**) were marked by monomeric red fluorescent protein. (**K**) Ofd1-GFP detected in a basal body-like pattern in the apical aspect of epithelia in the otic vesicle. (**L**) Otic vesicle of an embryo co-injected with Ofd1-GFP and 4 ng *ofd1* ATG MO showed no signal above background. The solid line outlines the vesicle in (K) and (L). (**M**–**P**) In the tail region, Ofd1-GFP signal (green in M) was detected in centrosomes, as confirmed by co-localization with γ-tubulin (red in N), and weakly in nuclei, as confirmed by counterstaining nuclei with DAPI (blue in O). The merged picture is shown in (P). (**Q**–**T**) Co-localization of Ofd1-GFP signal (green in Q) with γ-tubulin (red in R) at the apical surface of cells in the neural tube of 24 hpf embryos, as viewed from the dorsal aspect. Nuclei are stained blue in (S), with the merged picture shown in (T).

Table 1. Abnormal phenotypes in *ofd1* MO-injected embryos

	Ofd1 ATG MO 5 ng	*ofd1* SPL6 MO 4 ng
Curved body (%)	46	11
Hydrocephalus (%)	3	12
Ventricular malformation (%)	NA	44
Supernumerary otoliths (%)	20	30
Oedema (%)	33	27

Frequency of abnormal phenotypes in *ofd1* MO-injected embryos ($n = 75$ for ATG MO and $n = 135$ for SPL6). None of these defects were observed in similar numbers of controls.

the heart was, within a minute, followed by fluorescence appearing in the main circulation, including the dorsal aorta and posterior cardinal vein (Supplementary Material, Fig. S3). This technique can therefore be used to determine whether the dorsal aorta is present and also whether its lumen is patent and connected to the circulation. The same injections provide a method for assessing glomerular filtration because low molecular weight dextran should be filtered by normal glomeruli, with dextran then taken up by the proximal part of the pronephic tubule (38). Thus, visualization of particulate fluorescence over the pronephros is a marker of filtration. We also assessed glomerular morphology by analysing *wt1a* expression, a gene encoding a podocyte transcription factor (39,40) and by electron microscopy. In control embryos, injected at either 60 or 72 hpf, FITC-dextran rapidly appeared in the general circulation and underwent glomerular filtration, with fluorescence localizing in pronephric tubules from 20 min post injection up to 20 h, the end of the observation period (Fig. 3A, C and E and data not shown). In *ofd1* SPL6 MO (4 ng) injected embryos, while fluorescence rapidly entered and progressed around the circulation, its accumulation over pronephric tubules was minimal or absent even after 20 h (Fig. 3B, D and F and data not shown). In addition, *ofd1* MO-injected embryos (4 ng) showed significantly ($P < 0.0001$) impaired fusion of the two glomerular primordia at 48 hpf (45% of 74 embryos), 60 hpf (20% of 126) and 72 hpf (17% of 113) (Fig. 3H and J) when compared to controls ($n = 75$ 0% at 48 hpf; Fig. 3G and I). Furthermore, injection of *ofd1* ATG MO (5 ng) resulted in impaired fusion in 25% of the 57 embryos examined at 60 hpf, showing that this effect was not unique to the *ofd1* SPL6 MO. At 72 hpf, capillary loops in glomeruli of *ofd1* MO-injected embryos were less prominent than controls (Fig. 3K and L) and while glomerular endothelia were present in controls and *ofd1* MO-injected embryos, fenestrae, through which blood is filtered, were rarely detected in the latter (Fig. 3M and N). At 4 days, glomeruli in *ofd1* MO-injected embryos that developed oedema continued to lack morphologically normal capillary loops, and there was evidence of endothelial degeneration

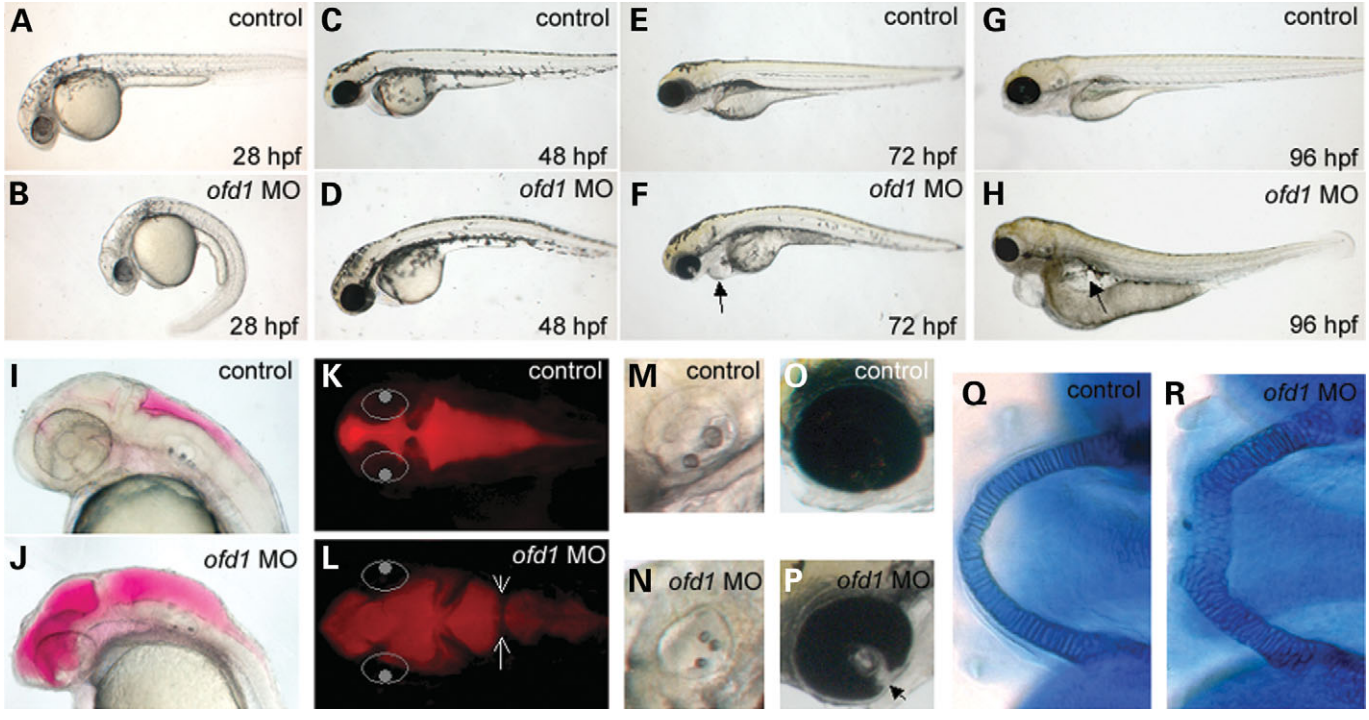

Figure 2. General dysmorphology of *ofd1* MO-injected embryos. (**A**, **C**, **E** and **G**) Lateral views of 28, 48, 72 and 96 hpf controls. (**B**, **D**, **F** and **H**) Time-matched 4 ng *ofd1* SPL6 MO-injected embryos. (B) An embryo injected with *ofd1* MO displaying bent body axis. (F) Pericardial oedema in an *ofd1* MO-injected embryo, indicated by the arrow. (H) Generalized oedema in an *ofd1* MO-injected embryo (arrow). (**I**–**L**) 30 hpf embryos injected with rhodamine-dextran into hindbrain ventricles. In (K) and (L), the eyes are indicated by white circles to help orientation. (I and K) Lateral and dorsal views of the fluid-filled ventricles (red) in controls. (J and L) Lateral and dorsal views of *ofd1* MO-injected embryo with widespread dilatation in the ventricular system. Note the abnormal tissue bridge in the hindbrain ventricle (arrows in L). (**M** and **N**) The control otic vesicle contained two otoliths (M), whereas three small otoliths were noted in this MO-injected embryo (N). (**O** and **P**) In 72 hpf controls, fusion of the retina in the optic cup is nearly complete (O) but a cleft (coloboma) was noted in this *ofd1* MO-injected embryo (arrowhead in P). (**Q** and **R**) Alcian blue stained lower jaws at 5 days post fertilization. In controls (Q), Meckel's cartilage cells are arranged in a column of cuboidal cells, forming a U-shaped structure. In contrast, in the *ofd1* MO-injected embryo (R), the structure was shorter and wider, and was composed of rounded cells.

(Fig. 3O–R). While a dorsal aortic lumen was evident in the section of glomeruli in a 72 hpf *ofd1* MO-injected embryos (Fig. 3L), a patent lumen was not observed in sections of glomeruli from a 96 hpf *ofd1* MO-injected embryos (Fig. 3P).

Laterality defects in *ofd1* MO-injected embryos

Embryos injected with *ofd1* MO showed a dose-dependent randomization of laterality of visceral organs and brain. Injection of *ofd1* ATG or SPL6 MOs (4 ng) produced reversal of heart jogging or midline hearts in ~20% of embryos. Injection of 5 ng caused complete randomization of laterality; looping was leftwards in 49%, rightwards in 43% and with no looping in the remainder, while in controls it was leftwards in 97% and rightwards in 3% (Fig. 4A–C). Using *ofd1* ATG MO (5 ng), the pancreas was left-sided in 57% and right-sided in 43%, whereas every control showed left-sided position (41) (data not shown). Nodal signalling controls vertebrate laterality (42) and expression of *nodal* pathway genes which are normally restricted to the left in zebrafish embryos (43–45), was altered in *ofd1* MO-injected embryos. At 20 hpf, *lefty1* (*lft1*) and *cyclops* (*cyc*) are both normally expressed in the left epithalamus and *lefty2* (*lft2*) as well as *southpaw* (*spaw*) are normally expressed in left lateral plate mesoderm (Fig. 4D, arrow, and data not shown). Injection of *ofd1* ATG MO (5 ng) or SPL6 MO (4 ng) disrupted normal patterns, consistent with randomization of situs, with excess right-sided, bilateral and absent expression (Fig. 4E–G, Table 2 and data not shown).

KV ciliary functions are disrupted in *ofd1* MO-injected embryos

In *ofd1* MO-injected embryos, a ciliated KV formed between 12 and 16 hpf (Fig. 5A and B) but cilia were shorter ($P < 0.0001$) than normal (Fig. 5C). To assess ciliary motility, beads were injected into KVs and followed as surrogate markers of intravesicular flow. In seven of eight control KVs, beads followed regular, anti-clockwise paths whereas bead trajectory was qualitatively abnormal in 6 of 10 *ofd1* MO-injected vesicles, deviating from a circular anti-clockwise path with loops and zig-zags (Fig. 5D and E and Supplementary Movies 1 and 2). Bead speeds were lower after *ofd1* MO injection (Fig. 5F; controls, 60 ± 11 μm/s, compared to *ofd1* MO-injected embryos, 45 ± 12 μm/s, $P = 0.02$). We assessed 10-somite stage KVs (Fig. 5G and H) by transmission electron microscopy. Though we observed many cilia we recorded only cilia that were at an appropriate sectioning angle, which allowed examination of axonemal structure. From a set of four control embryos of 52 cilia observed, eight had a $9 + 0$, one had a $9 + 1$, 42 had a $9 + 2$, and one had a $9 + 3$ configuration of axonemal doublets

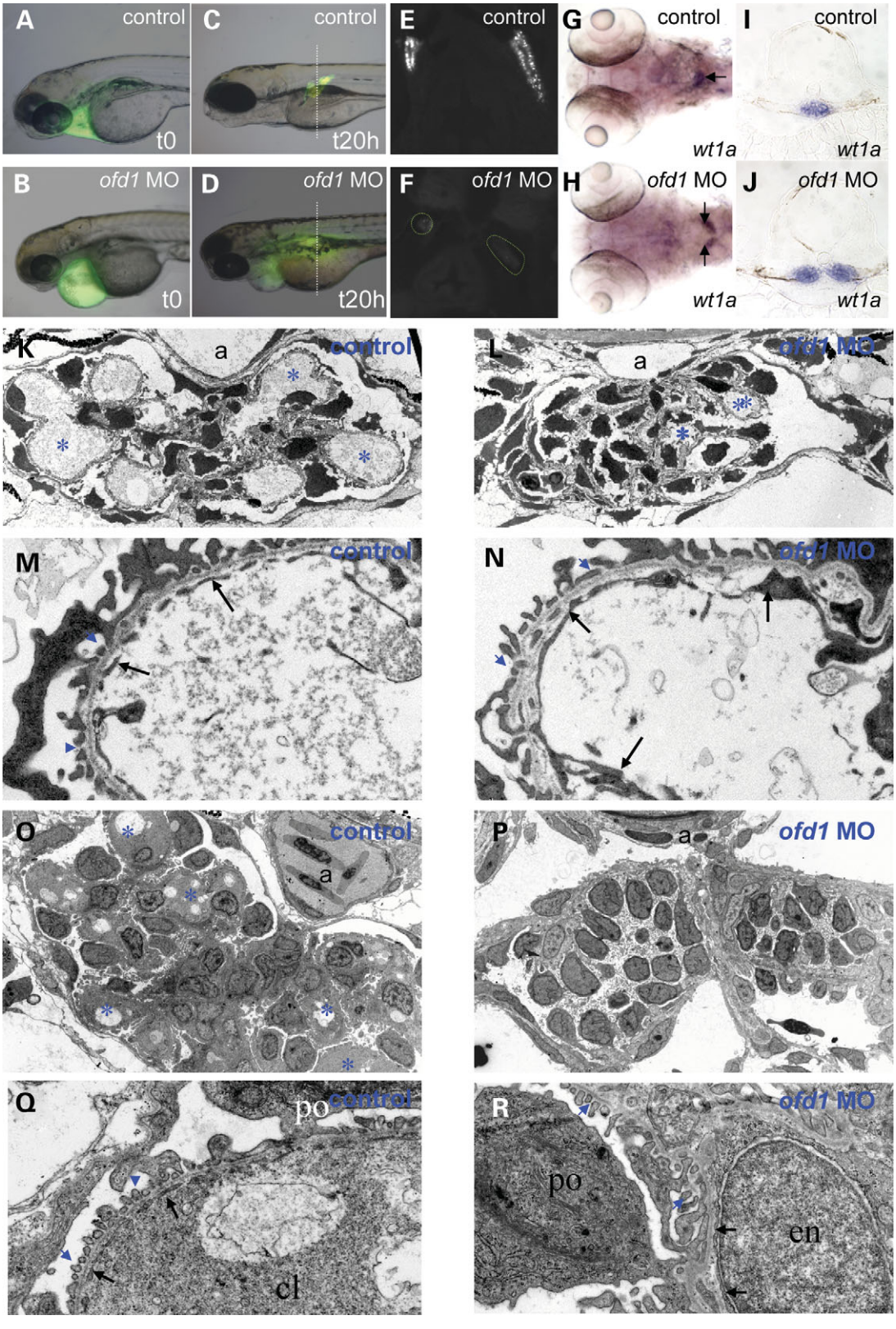

Figure 3. Glomerular function and structure in *ofd1* MO-injected embryos. (**A**–**F**) Control and *ofd1* MO-injected embryos treated with 10 kDa dextran injected into the pericardial space at 72 hpf to assess glomerular filtration. (A and B) Control and *ofd1* MO-injected embryos imaged immediately after injection. Fluorescence was detected in the pericardium. (C) 20 h after injection, dextran had been excreted from the circulation in live control embryos, and fluorescence was detected in proximal tubules after endocytosis of glomerular filtrate. (D) Time-matched *ofd1* SPL6 MO (4 ng) injected embryo in which fluorescence remained visible in the pericardium and systemically, but could not be detected in pronephric tubules. Note that the vertical lines in C and D represent the planes of section

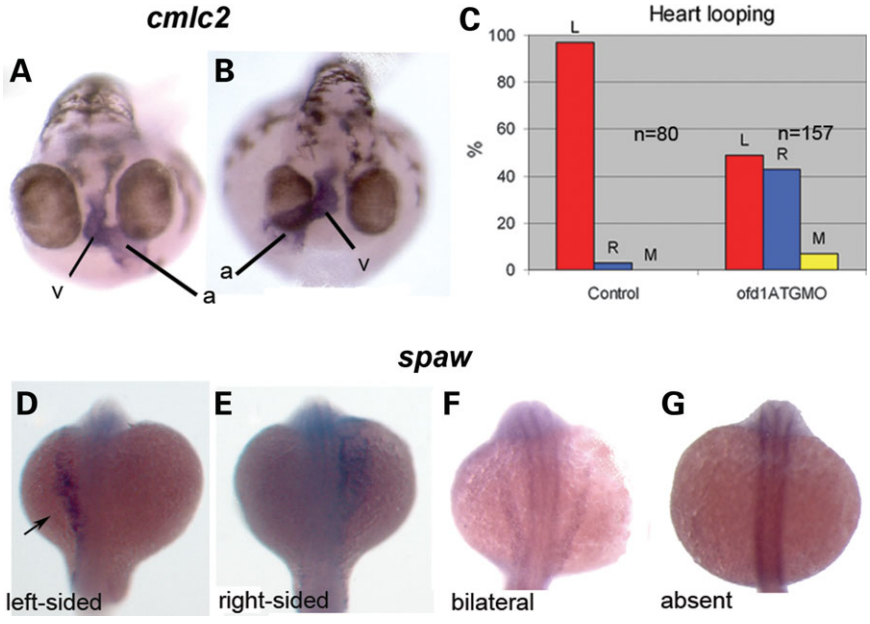

Figure 4. Left-right patterning is altered in *ofd1* MO-injected embryos. ISH for *cardiac myosin light chain 2* (*cmcl2*) was used to visualize the heart tube in 48 hpf embryos. (**A**) In wild-type embryos, the atrium (a) loops to the left (v), ventricle. (**B**) In this *ofd1* MO-injected embryo, the loop was reversed. (**C**) Frequencies of heart looping positions in 80 controls embryos and 157 embryos injected with *ofd1* ATG MO (5 ng). (**D**–**G**) In *ofd1* MO-injected embryos at 20 hpf (19-21 somites) *southpaw* (*spaw*) could be expressed either on the left only (D), on the right only (E), bilaterally (F) or could be absent (G). Arrow in (D) indicates expression in the left lateral plate mesoderm, the normal position.

Table 2. Analysis of *southpaw* expression in *ofd1* MO-injected embryos

MO	*n*	Left (%)	Right (%)	Bilateral (%)	Absent (%)
control	148	84.5	4.1	4.1	7.4
ofd1 ATG MO	86	24.4	23.3	26.7	25.6
ofd1 SP6 MO	91	72.5	11.0	7.7	8.8

Southpaw expression was assessed at 19–21 somite stage by ISH in controls and in embryos injected with 5 ng of *ofd1* ATG MO or 4 ng of SPL6 MO.

(Fig. 5I and J and data not shown). We found no control axonemes that were disrupted. From a set of four *ofd1* MO-injected embryos, of 27 cilia recorded, 10 were 9 + 0, 1 was 9 + 1, 7 were 9 + 2 and 9 contained disrupted or displaced doublets (Fig. 5K–N). Occasionally cilia in MO-injected embryos showed vesicles under the ciliary outer membrane (Fig. 5M and N).

CE movements are disrupted in *ofd1* MO-injected embryos

At the tailbud stage (10 hpf), directly before formation of the first somite, 50% of *ofd1* MO-injected embryos (4 ng SPL6 MO; $n = 66$) exhibited delayed anterior prechordal plate migration and a widened neural plate (Fig. 6A and B), phenotypes resembling *wnt11* mutants (30). Embryos injected with a low dose *ofd1* SPL6 MO (2 ng; $n = 13$), however, showed no migration defects, whereas 43% of *wnt11* MO (1 ng) injected embryos ($n = 16$) showed delayed migration. This defect was present in 13 of 14 embryos co-injected with low dose *ofd1* and *wnt11* MOs, a significant increase in comparison with *wnt11* MO alone ($P = 0.007$). Co-injected embryos had the widest neural plates (Fig. 6C–E). Homozygous *tri (vangl2)* mutant embryos have CE defects comprising shortened and widened somites and neural plates (28). At 7–8 somite stage, there was no significant difference in anterior neural plate widths between controls (155 ± 7 μm, $n = 7$) and low dose (2 ng) *ofd1* SPL6 MO-injected embryos (160 ± 10 μm, $n = 8$), while 2 ng *vangl2* MO-injected embryos had wider rhombomeres (230 ± 13 μm, $n = 10$) than controls, an effect significantly ($P = 0.006$) enhanced after co-injection with low dose *ofd1* MO (291 ± 7 μm, $n = 10$) (Fig. 6F–J). At this stage, embryonic axes were slightly but significantly ($P = 0.032$) shorter in *ofd1* MO-injected embryos compared with controls (775 ± 11 μm, $n = 8$ versus 816 ± 13 μm, $n = 7$). Injection of *vangl2* MO predictably generated shortened embryos (569 ± 10 μm, $n = 10$), while co-injection of *ofd1* MO produced a modest further shortening

depicted in (E) and (F). (E and F) Transverse sections of control and MO-injected embryos fixed at 20 h post injection. (**G**–**J**) *wt1a* ISH at 72 hpf. Note the fused glomerulus in the midline of the control (arrow in the whole mount in G) but two separate structures in the *ofd1* SPL6 MO-injected embryo (arrows in H). These two embryos are shown in transverse histological sections in (I) and (J). (**K**–**N**) Transmission electron microscopy of 72 hpf larvae. Low power (3000×) views show a control glomerulus (K) with prominent capillary loops (asterisks), and a glomerulus from an *ofd1* SPL6 MO-injected embryo with less prominent loops (L). Dorsal aorta (a) is evident in both control and *ofd1* MO-injected embryos (K and L). 25 000× magnification of control capillary loop (M) showing the thin endothelial cytoplasmic layer (arrows) interrupted by numerous gaps, or fenestrae, and of a MO-injected embryo capillary loop (N) with normal endothelia (arrows) but almost devoid of fenestrae. (**O**–**R**) Glomeruli at 4 days post fertilization. Low power views (3000×) in (O) and (P) and high power views in (Q) and (R) (25000×). In control glomeruli (O and Q), note numerous capillary loops (cl) (asterisks in O), a patent aorta (a) and fenestrated endothelia (arrows in Q). In *ofd1* MO-injected embryos (P and R), glomeruli lacked loops and a patent aorta (P) and endothelia (arrows in R) lacked fenestrae; podocytes (po), however, had grossly normal foot processes (blue arrowheads in R). Some endothelial nuclei (en) appeared amorphous and swollen.

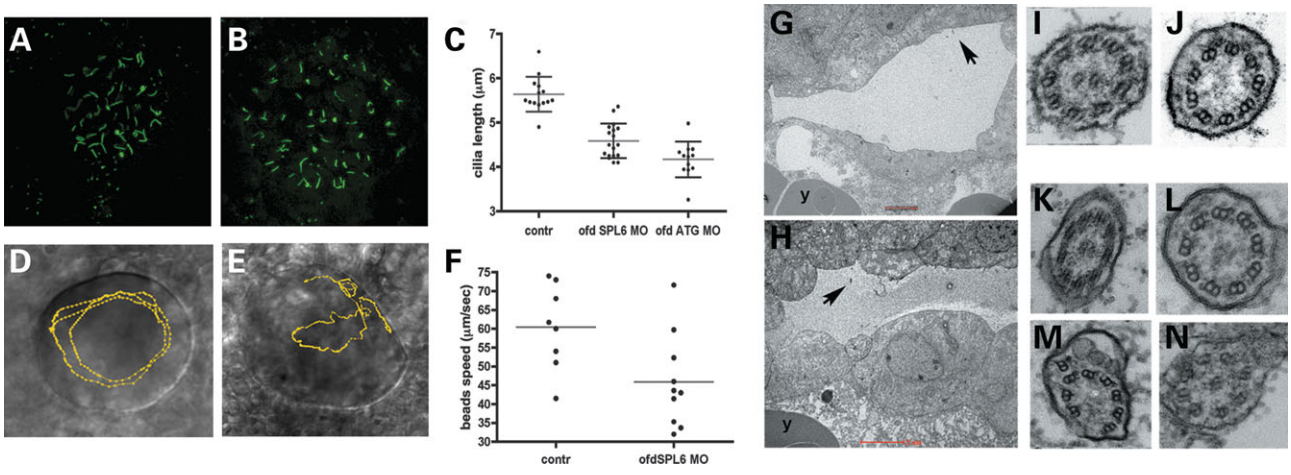

Figure 5. Effects of *ofd1* MOs on KV cilia and intravesicular flow. (**A** and **B**) Cilia in KVs of 10 somite control embryos (A) and *ofd1* MO-injected embryos (B) visualized after immunostaining (green) for acetylated α-tubulin. (**C**) Plots of cilia lengths in KVs. Each dot represents the average size of all cilia in a single vesicle. Note that both the *ofd1* SPL6 and ATG MOs cause significant reductions in length. (**D** and **E**) Injected beads were tracked using video microscopy. (D) KV of a control embryo: beads follow an anti-clockwise circular path (yellow line). (E) KV of an *ofd1* SPL6 MO (4 ng) injected embryo where beads had irregular trajectories, characterized by loops and zig-zags (yellow line). (**F**) Average bead speed/KV was reduced in *ofd1* MO-injected embryos. (**G** and **H**) Ultrathin sections showing a 10-somite stage KV in control (G) and in an *ofd1* ATG MO (5 ng) injected (H) embryo. Arrows indicate cilia and 'y' marks the yolk. (**I**–**N**) Transmission electron micrographs show transverse sections of KV cilia. Both 9 + 2 and 9 + 0 arrangements of axonemal microtubules were seen this control KV (I and J) and in a vesicle of an embryo injected with *ofd1* MO (K and L). Cilia with inclusions under the membrane and/or disrupted axonemal microtubules were detected after MO injection (M and N).

(534 ± 7 μm, $n = 8$) (Fig. 6F–I). At 60 hpf (Fig. 6K–O), there was no significant difference between *ofd1* MO-injected embryos and controls, whereas co-injected embryos were significantly ($P = 0.0004$) shorter than *vangl2* MO-injected embryos (1550 ± 17 μm, $n = 25$ versus 1670 ± 25.5 μm, $n = 21$).

Tri/Vangl2 and Ofd1 both regulate glomerular fusion

We examined glomerular fusion in *vangl2* MO-injected embryos and in *tri/vangl2* mutants, either with or without injection of *ofd1* MO (Fig. 6P–T and data not shown). At 60 hpf, all 54 control embryos showed normal glomerular fusion. By contrast glomerular fusion failed in 20% of the 63 *ofd1* SPL6 MO (4 ng) injected embryos.

In *vangl2* MO (2 ng) injected embryos glomerular fusion failed in 5 of 20 individuals ($P = 0.001$ versus controls). Glomerular fusion failed in 63% of 51 *tri* mutant embryos and in 7% of the 106 otherwise phenotypically wild-type siblings.

We performed FITC-injections into *tri* mutant embryos at 60 hpf and found that all had a patent dorsal aorta (data not shown). Injection of *ofd1* SPL6 MO (4 ng) into *tri* mutant embryos led to a failure of glomerular fusion in all 27 embryos, displaying a very wide glomerular separation, while 55% of the 82 siblings showed failed fusion. Knockdown of Ofd1 thus led to significantly increased fusion defects in *tri* mutant ($P = 0.001$) and sibling ($P < 0.001$) embryos. We also performed FITC-injections into *tri* mutant embryos, which had been injected with *ofd1* MO and found that 8 of 13 lacked a patent dorsal aorta (data not shown).

Gene expression analyses in *ofd1* MO-injected embryos

Because of links between Ofd1, cilia and Shh signalling in mice (21–24), we performed ISH for genes upregulated by Hh signalling (46–49). Embryos injected with *ofd1* MO showed overtly normal expression patterns of *ptc1* in somites (adaxial cells) and ventral brain, *nkx2.2* in diencephalon, tegmentum, ventral hindbrain, spinal cord and pancreas, and *engrailed* in midbrain–hindbrain boundary and muscles pioneers (not shown). Real-time RT–PCR for *ptc1* and *ptc2* at mid-segmentation stage revealed no differences between controls and *ofd1* MO-injected embryos (not shown). We also measured gene expression in mid-gastrulation embryos using microarrays. Table 3 lists genes up- or down-regulated >2-fold in *ofd1* MO-injected embryos (see Supplementary Material, Table S1 for the complete set) and we verified changed expression of selected genes by real-time RT–PCR (Fig. 7). Strikingly, in the microarray study, the greatest-fold upregulated transcript was *ofd1* itself. We also noted a 2-fold downregulation in *ankyrin repeat domain 6* (*diversin*), which modulates zebrafish CE and non-canonical Wnt signalling (50,51).

DISCUSSION

Using zebrafish to investigate the function of the gene mutated in OFD1 syndrome, we have helped to elucidate roles for this protein in the regulation of cilia function, cell movements and other developmental processes. Transcription of *ofd1* occurs ubiquitously in embryos with noticeably higher levels in ciliated organs such as otic vesicles and neuromasts (52,53). By analysing Ofd1-GFP localization in live embryos, we conclude that zebrafish Ofd1, like human OFD1 (6,7), resides in basal bodies and centrosomes. Fluorescence did not extend from basal bodies, making it unlikely that Ofd1 is also associated with axonemes in ciliary stalks. In fixed samples, we additionally observed low levels of Ofd1-GFP in nuclei, consistent with the nuclear localization of OFD1 reported in mammalian Cos-7

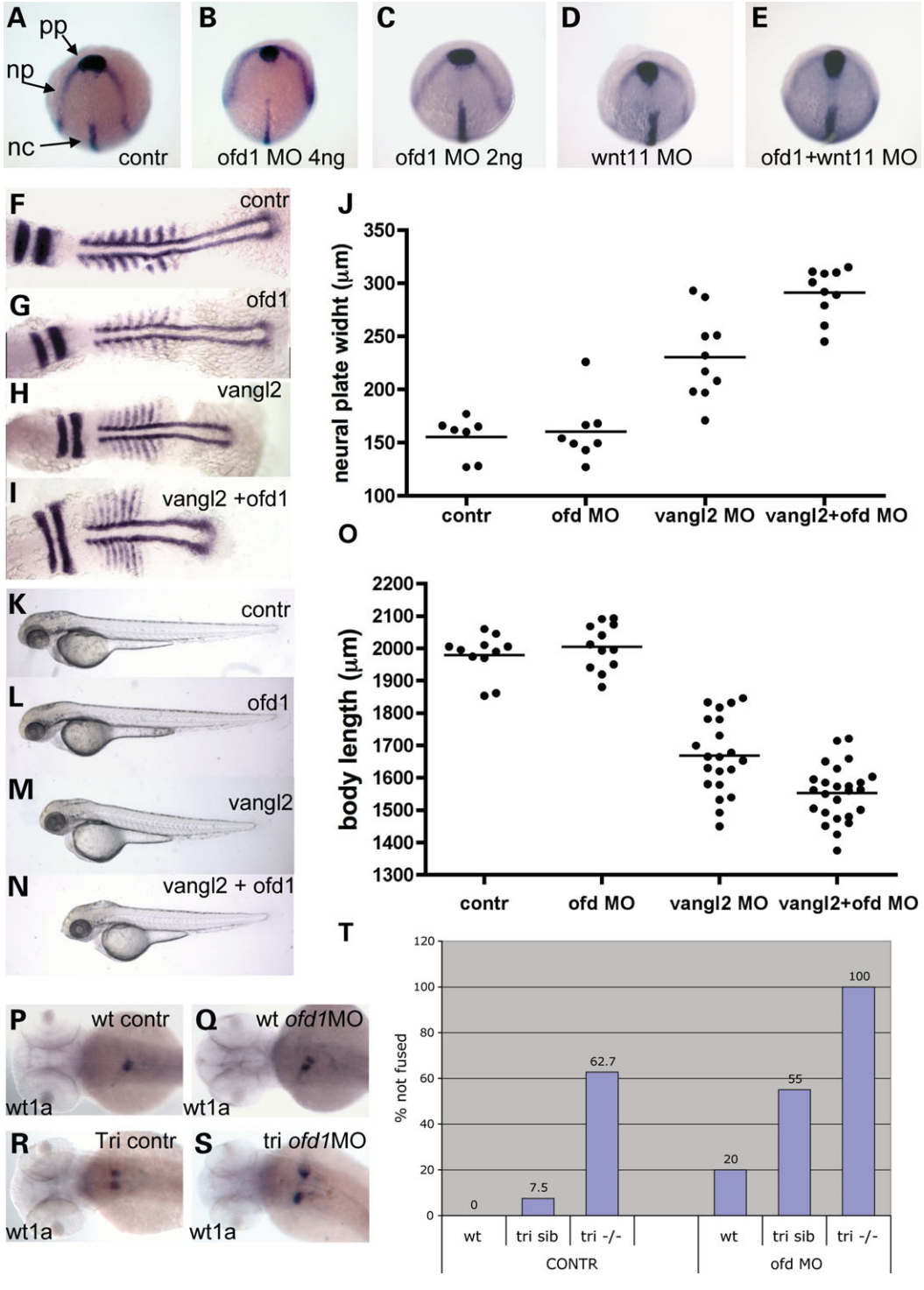

Figure 6. CE failure in *ofd1* MO-injected embryos. (**A**–**E**) Tailbud stage embryos hybridized with a cocktail of riboprobes: *hgg1* as a marker for prechordal plate (pp), *dlx3* as a marker for anterior margin of the neural plate (np) and *ntl* as a notochord (nc) marker. pp migration was delayed and the neural plate was wider in some embryos injected with 4 ng *ofd1* SPL6 MO (B), but not in those injected with 2 ng only (C). Similar CE defects were observed in a subset of *wnt11* MO-injected embryos (D), while all embryos showed the defects upon co-injection (E). (**F**–**I**) Embryos at the seven-somite stage hybridized with riboprobes for *myoD*, a marker of somite and adaxial cells, and *krox20*, a marker for rhombomeres 3 and 5. Representative embryos are shown: control (F), injected with *ofd1* SLP MO (G), injected with *vangl2* MO (H) and co-injected (I), with neural plate widths shown in (**J**). Note that co-injection of low dose *ofd1* MO with *vangl2* MO accentuated rhombomere widening and axis shortening versus *vangl2* MO-injected embryos (see *Results* text for details). (**K**–**O**) When assessed at 60 hpf, *ofd1* and *vangl2* MO co-injected embryos had shorter bodies than those injected with *vanlg2* MO alone (see *Results* text for details). (**P**–**S**) *wt1a* ISH to detect glomeruli at 60 hpf. Note the fused glomerulus in controls (P), with examples of failed fusion in wild-type embryos injected with *ofd1* SPL6 MO (4 ng) (Q), *tri* mutants without (R) or with (S) *ofd1* SP6 MO (4 ng); note the extreme separation of glomeruli in the latter condition. (**T**) Frequencies of failed fusion: note the accentuation of failed fusion in *tri* siblings upon injection of *ofd1* MO.

Table 3. Genes up- and downregulated >2-fold in *ofd1* ATG MO-injected embryos at shield stage

Ensembl ID and description	ZFIN ID	FC	Function
ENSDARG00000000529:oral-facial-digital syndrome 1	ZDB-GENE-030131-5427	4.323	Centrosome/basal body function
ENSDARG00000004232:Delta-like protein B precursor	ZDB-GENE-980526-114	3.362	Notch signalling pathway
ENSDARG00000006604:Poliovirus receptor-related protein 3 precursor	ZDB-GENE-050327-14	2.471	Negative regulation of signal transduction
ENSDARG00000043638:Tom1l2 protein (Fragment)	ZDB-GENE-060721-1	2.549	Intracellular protein transport
ENSDARG00000056114: Rap2 interacting protein	ZDB-GENE-040426-842	2.472	Small GTPase regulator activity
ENSDARG00000014794:hypothetical protein LOC436930	ZDB-GENE-040718-405	2.460	Ubiquinol-cytochrome c reductase core protein II
ENSDARG00000057114:zgc:101819	ZDB-GENE-030131-740	2.279	Uncharacterized protein
ENSDARG00000040344:linker histone H1M	ZDB-GENE-030131-5614	2.185	Nucleosome assembly (germline-specific)
ENSDARG00000025641:GLI-Kruppel family member GLI2a	ZDB-GENE-990706-8	2.089	Transcription factor activity
ENSDARG00000005039:glutathione S-transferase pi	ZDB-GENE-020806-4	2.058	Glutathione transferase activity
NA	ZDB-GENE-040718-248	2.021	Vertebrate transmembrane 4 superfamily-like
ENSDARG00000034539:ras homolog gene family, member E Rho family GTPase 3a	ZDB-GENE-010319-40	2.035	Small GTPase mediated signal transduction
ENSDARG00000029370:ankyrin repeat domain 6	ZDB-GENE-030916-4	−1.937	Negative regulation of Wnt receptor signalling pathway
ENSDARG00000035507:Wu:fc62b08 protein (Fragment)	ZDB-GENE-030131-3973	−2.009	Probable ATP-dependent RNA helicase DDX3
ENSDARG00000057683:PREDICTED: similar to DNA replication licensing factor MCM6 (Mis5 homolog)	ZDB-GENE-030909-6	−2.071	DNA helicase activity
ENSDARG00000007216:ATP-binding cassette, sub-family E (OABP), member 1	ZDB-GENE-040426-1995	−2.098	Ribonuclease inhibitor activity
ENSDARG00000011235:Homeobox protein OTX2 (ZOTX2)	ZDB-GENE-980526-406	−2.522	Transcription factor activity
ENSDARG00000012076:Apolipoprotein A-I precursor (Apo-AI) (ApoA-I)	ZDB-GENE-990415-14	−2.609	Cholesterol transporter activity
ENSDARG00000041685: similar to alpha-2 microglobulin-1	NA	−2.684	Protease inhibitor activity
ENSDARG00000056314:PREDICTED: similar to alpha-2-macroglobulin-1	NA	−2.534	Protease inhibitor activity
ENSDARG00000016771:transferrin-a	ZDB-GENE-980526-352	−4.881	Iron ion transport activity

Ensembl ID and description for the genes that are up- or downregulated more than 2-fold (in green and red respectively) in *ofd1* MO-injected embryos are given in the first column, ZFIN IDs in the second, fold changes (FC) are listed in the third column and a short description of the protein function is given in the fourth column. FC are an average of the values from spots for the same probe on the microarray. Only values with an adjusted *P*-value <0.05 were considered.

cells; in these cells, OFD1 co-immunoprecipitates with a chromatin remodelling complex (8). In zebrafish embryos injected with *ofd1* ATG MO, the most upregulated gene at mid-gastrulation was *ofd1* itself, confirming this MO induced a specific response and also suggesting that levels of *ofd1* transcript are regulated by the amount of available Ofd1 protein. Collectively, these observations raise the possibility that Ofd1/OFD1 might regulate transcription.

Ofd1, ciliary function and lateralization

Each of three *ofd1* MOs produced a similar spectrum of phenotypic traits, including a curved body and laterality defects that resemble other zebrafish mutants with disrupted ciliary functions (52,54,55). Although KVs were ciliated in *ofd1* MO-injected embryos, their cilia were shorter than normal, and we deduced that intravesicular flow was slowed and irregular based on the movement of injected beads. These data are consistent with the notion that OFD1 syndrome is indeed a ciliopathy. Further studies are needed to establish mechanism of these ciliary anomalies but, based on the structural anomalies of KV cilia in *ofd1* MO-injected embryos, we suggest that Ofd1 in basal bodies facilitates the biogenesis of ciliary axonemes and/or is needed to maintain these structures.

The mouse embryonic node has been reported to contain motile cilia (15). Electron microscopy demonstrated the presence of cilia with a 9 + 0 configuration (15). Subsequently, two populations of cilia in the mouse node were described (56). One population of cilia was found to express dynein, is considered to be actively motile and to generate leftward flow, while the other population lacks dynein and is thought to sense flow (56). Until the current study, only 9 + 2 cilia have been described in zebrafish KVs (57,58) but in both control and *ofd1* MO-injected embryos, we found profiles with 9 + 2 or 9 + 0 arrangements. In both types of cross-section, dynein arms associated with the outer microtubules were present. Moreover, some KV cilia had deranged ultrastructure and occasional inclusions under the membrane after dowregulation of Ofd1. These ultrastructural abnormalities, together with the significant shortening of cilia, serve to explain the perturbed flow following administration of *ofd1* MOs. A reduction of Ofd1, therefore, probably renders KV cilia unable to generate adequate flow to efficiently assign laterality. Indeed, the reversed heart jogging/looping in zebrafish embryos with reduced Ofd1 was preceded by disruption of expression of genes normally restricted to the left side of the body. Whether Ofd1 is also required to mediate possible sensory functions in KV cilia, remains to be established.

Cilia are absent in mammalian cells without functional Ofd1 (23,24), including those in the embryonic node. With regard to the *ofd1* ATG MO, we noted that while it was

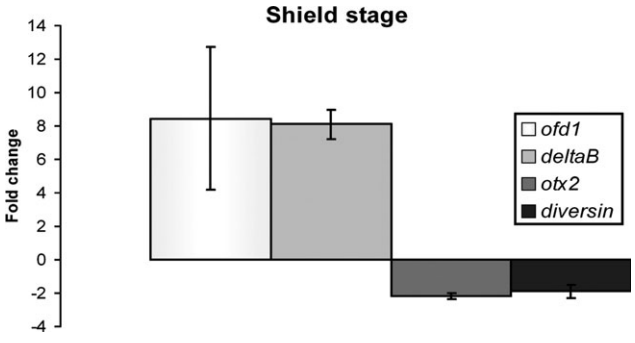

Figure 7. Validation of microarray data using real time RT–PCR. Fold-changes in levels of expression for *ofd1*, *deltaB*, *otx2* and *diversin* in embryos injected with 5 ng of *ofd1* ATG MO and collected at shield stage. Results depict the average and standard deviations of three different experiments.

sufficient to ablate the expression of Ofd1-GFP (Fig. 1L), cilia, albeit of abnormal length and function, were still present in KVs of MO-injected embryos. However, in the absence of an antibody to detect endogenous zebrafish Ofd1 protein, we cannot exclude the possibility that we have only disrupted expression of a fraction of Ofd1 protein. Very high doses of MO, which may have generated more extreme downregulation of endogenous Ofd1, were associated with a generalized toxicity, precluding further analyses of the KV. Another possible explanation is that zebrafish possess other *ofd1*-like genes. The initial description of the zebrafish homologue of human *OFD1* noted only one form of the zebrafish *ofd1* gene (11). Using Exonerate (http://www.ebi.ac.uk/~guy/exonerate/) (59) to scan the latest assembly of the zebrafish genome, we found only one *ofd1* gene. Moreover, in TreeFam (http://www.treefam.org/) (60), there is no indication of any duplication.

In *ofd1* SPL MO-injected zebrafish embryos, diminished amounts of normal *ofd1* message were still present, yet cilia were present, albeit shorter than normal and dysfunctional. If we assume that the abnormally spliced *ofd1* transcript did not result in a dominant negative effect, these data are consistent with the notion that downregulation, rather than complete absence, of Ofd1 can significantly perturb ciliary ultrastructure and function. If there is a critical level of Ofd1 below which its functions fail, this helps to explain why XX women carrying one mutated *OFD1* allele have the clinical syndrome (11). To date, there have been no published studies, which have sought and studied cilia in women with OFD1 syndrome. In a unique human family in which X-linked recessive mental retardation co-segregated with a frameshift mutation in *OFD1*, affected males had severe respiratory tract infections and although cilia were seen in respiratory epithelia, their motility was poorly co-ordinated (61). These features in human epithelia parallel our observations of KV ciliary defects in zebrafish depleted of Ofd1.

In some *ofd1* MO-injected embryos, we observed dilated brain ventricles, reminiscent of malformations in human OFD1 (5). This could indicate the defective functioning of the motile cilia that circulate cerebrospinal fluid (62–64). We detected cilia on the ventricular surfaces of *ofd1* MO-injected embryos (data not shown) but did not assess them further because in several such embryos, we detected tissues bridges in the brainstem ventricle, consistent with incomplete opening (65) and raising the possibility that morphogenetic problems contributed to the ventricular dilation. Our observations that Ofd1 depletion could generate abnormal otoliths is consistent with similar anomalies noted in other zebrafish mutants with ciliary phenotypes (52,66) and with hearing loss reported to occur in 7% of OFD1 females (67). Finally, with respect to retinal colobomas found in a subset of *ofd1* MO-injected embryos, we note that OFD1 females occasionally have 'retinal atrophy/thin optic nerves' (67).

Ofd1, CE, ciliary function and Wnt signalling

Our data implicate, for the first time, Ofd1 in CE during gastrulation, consistent with other studies linking cilia and non-canonical Wnt signalling (24,36). This conclusion is supported by the finding that Ofd1 downregulation enhanced the phenotype of embryos that were also disrupted for *wnt11* or *vangl2*, genes coding for PCP proteins known to be important for CE (30,33). Similar interactions have been shown for several *bbs* genes coding for basal body proteins (34). As suggested for Inversin, another basal body protein (17), Ofd1 might influence the switch from the canonical β-catenin to the non-canonical, PCP, Wnt pathway. This could be an indirect result of a requirement for Ofd1 in normal ciliary structure and function, or could occur directly through interaction with Wnt signalling components, as described for the ciliary protein Seahorse/Lrrc6l (68). Indeed a recent paper reported that *Ofd1* null mouse embryonic stem cells lack cilia and are hyper-responsive to Wnt ligand, showing exaggerated β-catenin signalling (24). Of extra interest, we found that *ofd1* MO injection downregulated *diversin*, a gene known to regulate zebrafish gastrulation movements (51) and that has functional overlap with *inversin*. We suggest that compromised CE might be more widely observed in zebrafish 'ciliary' mutants if such phenotypes are specifically analysed.

Glomerular fusion as a manifestation of CE

The effects of *ofd1* knockdown on the pronephros are probably complex but we consider that the most interesting 'renal observation' is the delayed glomerular fusion, which we suggest is a CE defect. This idea is supported by our observation that there was a significant incidence of fusion failure after *vangl2* disruption, an effect that was enhanced in embryos where both *vangl2* and *ofd1* were downregulated. Certain midline mutants show compromised glomerular fusion and, in these embryos, glomerular vascularization is also compromised because of morphological defects of the dorsal aorta (69). This prompts the question of whether an absent aorta is required to generate failed glomerular fusion in embryos injected with *ofd1* MO. Indeed, a dorsal aortic lumen was not apparent in sections (Fig. 3P) of a 96 hpf *ofd1* MO-injected embryo, although a lumen was apparent in the section of glomeruli in an 72 hpf MO-injected embryo (Fig. 3L). In fact, at 60 hpf, simply by observing anaesthetized embryos under the microscope, we always saw blood cells flowing through the dorsal aorta of both controls and *ofd1* MO-injected embryos (data not shown), and FITC-dextran injected into the pericardial space at 60 hpf was seen to circulate through the dorsal

aorta of both control and *ofd1* MO-injected embryos. In *tri* mutants, we always observed patent dorsal aortas at 60 hpf, whereas in *tri* mutants injected with *ofd1* MO, all of which showed marked fusion defects, a patent dorsal aorta was only detected in about a half. Taken together, these data show that the glomerular fusion defects noted at 60 hpf in *ofd1* MO-injected embryos, and in *tri* mutant embryos, occur in the presence of a patent dorsal aorta. Furthermore, the fact that all *tri* mutants injected with *ofd1* MO had very widely spaced glomeruli at 60 hpf, whereas only half of them had a non-functional dorsal aorta, is consistent with the explanation that we are observing additive CE defects from *ofd1* and *vangl2* depletion. Finally, while zebrafish *shh* and *gli2* mutants have failed glomerular fusion (69), we detected no downregulation of Hh target genes in *ofd1* MO-injected embryos.

Glomerular ultrastructure and filtration in *ofd1* MO-injected embryos

While the glomeruli of *ofd1* MO-injected embryos contain some capillary loops at 72 hpf (Fig. 3L), glomeruli visualized at 96 hpf appeared to lack patent capillaries. Thus, between 72 and 96 hpf, disruption of Ofd1 is associated with structural defects in glomerular vasculature, which would be predicted to severely reduce or preclude filtration, and these observations may in part explain the fact circulating FITC-dextran did not appear in pronephric tubules. Furthermore, at 72 hpf, glomerular endothelia in *ofd1* MO-injected embryos lacked the fenestrae through which blood would be filtered. One possibility is that glomerular capillary regression could be explained by reduced aortic perfusion associated with structural heart defects, themselves caused by *ofd1* MOs. Indeed, in 96 hpf *ofd1* MO-injected embryos, which had developed severe generalized oedema, circulation was absent (data not shown). Interestingly, zebrafish *floating head* (*flh*) mutant, which has a defective homeobox gene essential for notochord formation (69), also contains glomeruli with endothelia with fewer fenestrae than normal. The mouse *flh* homologue, *noto*, is essential for node morphogenesis and ciliogenesis in the posterior part of the notochord. Mutant mice display laterality defects and shorter cilia with irregularities in the axonemal structure but pronephroi were not studied (70). Surprisingly, in view of the occurrence of glomerular cysts in humans and mice with *OFD1/Ofd1* mutations (3,23), we did not see similar lesions in *ofd1* MO-injected fish embryos. However, we found that glomeruli in *ofd1* MO-injected embryos failed to filter low molecular weight dextran and we therefore deduce that impaired glomerular filtration probably contributed to the pericardial and systemic oedema. It is interesting to note that *tri* mutants with defective glomerular fusion do not develop oedema; therefore, the two phenomena do not seem to be related. Primary cilia in mammalian kidneys are thought to transduce a signal from tubular flow, which somehow prevents epithelial overgrowth into cysts (17–19). We reason that, in the absence of glomerular filtration and hence fluid flow, glomerular cysts will not form even if Ofd1 functions are disrupted. We detected cilia in the pronephric tubules of *ofd1* MO-injected embryos (data not shown) but did not analyse them further (e.g. for motility and length) because we failed to find a gross cystic phenotype in the pronephros.

MATERIALS AND METHODS

RT–PCR

Total RNA was extracted from embryos at different stages with Trizol and 500 ng was used for cDNA synthesis primed by random primers and performed with Superscript II RT (Invitrogen). The cDNA was then amplified according to standard protocols using *Taq*-DNA polymerase (Promega) in an Applied Biosystems 9700 (Gene Amp) thermocycling machine. PCR primers were manufactured by SIGMA or Operon. Primers used to detect cDNA expression are:

Fsue4: 5′-GTGATGTTCTGCAGATCATG
Rsue6: 5′-CTATAGAGGTGGTTTGAGTTG

To assess the effect of *ofd1* SPL6 and *ofd1* SPL7 MO on splicing, the following primers pairs were used respectively:

5F: 5′-TCTGAAGAGCTTGTTGATGG
7R: 5′-TTCTCTCGACTGATCAGAGC
FSUE7: 5′-GAAATCCTGGAGCTCAGACG
Rsuint7: 5′-CCTAATAACACTTGTCATGAGC

Maintenance of zebrafish

Breeding zebrafish (*Danio rerio*) lines were maintained at 28°C on 14 h light/10 h dark cycle. Fertilized eggs were obtained from natural spawning and grown in incubators at a temperature between 22 and 32°C depending on the stage required. Embryos were staged according to standard references (71). When necessary, formation of pigment was blocked by incubating embryos in 0.2 mM 1-phenyl-2-thiourea (PTU) at 24 h onwards. For imaging purposes, live embryos were manually dechorionated with no. 5 watchmaker's forceps, when necessary were anaesthetized with 0.02% tricaine (3-amino benzoic acid ethyl ester), and mounted for viewing in 3% methylcellulose in fish tank water. Pictures were taken using the following equipment: Nikon SMZ1500 dissecting scope, Leica DFC 320 digital camera and Leica Firecam software, if not otherwise stated.

MO and mRNA injections

The following Morpholino antisense oligonucleotides were ordered from Genetools:

ofd1 SPL6 MO: 5′-ATCTTCTCTACTGCAACACACATAC
5 mis *ofd1* SPL6 MO: 5′-ATgTTgTCTACTGgAAgACAg ATAC
ofd1 ATG MO: 5′-CTCCCTCTTTACTCGCAGACATGA
ofd1 SP7 MO: 5′-GTGCTTGTTTAATACCTCCTGGTGT
vangl2 MO: 5′-GTACTGCGACTCGTTATCCATGTC
wnt11 MO: 5′-GAAAGTTCCTGTATTCTGTCATGTC

They were diluted in Danieau's solution (5 mM HEPES pH 7.6, 58 mM NaCl, 0.7 mM KCl, 0.4 mM $MgSO_4$, 0.6 mM $Ca(NO_3)_2$) and the stated amount was injected in one to two cell stage embryos. Needles were pulled from glass capillary

tubes using a Clark Electromedical Instruments needle puller and injections were performed using a Picospritzer microinjector.

For mRNA injections, the Ofd1-GFP plasmid was obtained cloning the coding sequence of Ofd1 (from clone AI883216) in frame with the GFP sequence in the vector pCS2+, and the mRNA was synthesized with SP6 using the Promega kit. 100 pg of capped mRNA were injected at the one-cell stage.

ISH, immunolabelling and imaging

Embryo were fixed at the appropriate stage in 4% paraformaldehyde in PBS overnight at 4°C prior to undergo ISH or immunolabelling. Whole-mount *in situ* hybridization reactions were carried out according to published protocols (72). Sections from whole-mount *in situ* were cut after embedding stained embryos in JB4 resin (Polyscience Inc.). As a template for the *ofd1* probe transcription, a PCR fragment was amplified from 2-cell stage cDNA with the following primers:

T3*ofd1*Cter: 5′-GCaattaaccctcactaaagggCCCCTTCTCCAGCAGAGAGA

T7*ofd1*Cter: 5′-GCgtaatacgactcactatagggcCCCCAGAAATCATCGTCGGC

The antisense *ofd1* probe for ISH was transcribed using T7 polymerase and the sense probe using T3 polymerase.

Probes for wt1a, cmcl2, pdx1, lefty1, lefty2, southpaw, cyclops, ptc1, nkx2.2, engrailed, chordin, hgg1, dlx3, ntl, myoD and krox20 were obtained amplifying PCR fragments.

For fluorescence immunohistochemistry, primary antibodies were purchased from SIGMA. Mouse anti-γ-tubulin was used at a 1:500 dilution and mouse anti-acetylated α-tubulin at 1:800. The following secondary antibodies were used: Alexa-488 goat anti-rabbit IgG (A-11034, Molecular probes), Alexa-633 goat anti-mouse IgG (A-21050, Molecular probes), Alexa-488 goat anti-mouse IgG (A-11001, Molecular probes). Embryos were processed as previously described (58) and mounted with Vectashield Mounting Media with DAPI (Vector laboratories). Cilia labelled with anti-acetylated α-tubulin antibody were imaged at the confocal microscope using a 40× oil immersion objective and measurements were performed with Volocity software (Improvision) on the maximum projection obtained from the z-scans. Confocal images were acquired using a Leica SP5 confocal microscope.

Dextran injection in the brain and in the heart

For the glomerular filtration assay 2 nl of 10 mg/ml Lysine fixable fluorescein-conjugated dextran, 10,000 MW (D-1820 Molecular Probes) were injected in the pericardium of live fish while to visualize brain ventricle structure 2 nl of 100 mg/ml rhodamine-conjugated dextran, 70,000 MW (D1819, Molecular Probes) were injected in the hindbrain ventricle and images acquired at the fluorescence dissecting scope (Leica MZFL). After injection of dextran in the heart, some embryos were embedded in JB4 resin (Polysciences Inc.) and sectioned. Plastic sections were photographed using an Axioplan 2 Zeiss fluorescence microscope and Openlab software (Improvision).

Injection of beads in KV

0.5 nl of 0.02 μM diameter fluorescent microspheres (Molecular probes Fluospheres, F8787) diluted 1:20 in Danieau's solution were injected into the KV of 6 somite stage live embryos mounted in 1.5% agarose. Movement of the beads was observed and recorded using Volocity acquisition software and Axioplan 2 Zeiss fluorescence microscope. Beads tracking and speed calculation were performed with Volocity 4.0 software.

Alcian blue staining

Larvae at 5 days post fertilization were fixed overnight in 4% PFA, washed in PBS 0.1% tween and then transferred in the alcian blue solution (0.1% alcian blue, 80% ethanol, 20% acetic acid) overnight. On the next day, they were rehydrated through decreasing ethanol concentration in PBS, and left 1–3 h in a solution of 0.05% trypsin in 30% saturated sodium tetraborate. To remove pigmentation, larvae were bleached in 3% H2O2, 1% KOH for 2 h and then stored in 70% glycerol 1% KOH.

Electron microscopy

Embryos were immersed in freshly prepared primary fixative containing 2% PFA with 2% GA in 0.1 M sodium cacodylate buffer (pH 7.42) with added 0.1 and 0.05% magnesium and calcium chloride, respectively, at 20°C for 10 min before transferring to an ice bath for the remainder of 1 h. The samples were rinsed three times for 10 min each in sodium cacodylate buffer with added chlorides on ice. Secondary fixation with 1% osmium tetroxide in sodium cacodylate buffer only was carried out at room temperature for 1 h. All following steps were performed at room temperature. Embryos were rinsed three times in cacodylate buffer over 30 min and mordanted with 1% tannic acid for 30 min followed by a rinse with 1% sodium sulphate for 10 min. The samples were dehydrated through an ethanol series 20, 30 (staining en bloc with 2% uranyl acetate at this stage), 50, 70, 90 and 95% for 20 min each then 100% for 3 × 20 min. Ethanol was exchanged for propylene oxide (PO) for 2 × 15 min followed by 1:1 PO to Epon resin mixture for at least 1 h and neat Epon (with a few drops of PO) over night. The embryos were embedded in a flat moulded tray with fresh resin and cured in an oven at 65°C for 24 h. Sections of 8 nm were cut on a Leica UCT ultramicrotome, contrasted with uranyl acetate and lead citrate and imaged on an FEI 120 kV Spirit Biotwin using an F415 Tietz CCD camera.

We examined seven KVs from control embryos and five KVs from *ofd1* MO-injected embryos. We excluded from our analysis cilia with degradation of the peripheral ciliary membrane, which was the most common artefact, seen in up to a third of controls and MO-injected embryos.

Microarray analysis

Danio rerio sequences were selected from public full-length cDNA sequences (RefSeq), VEGA or ENSEMBL transcripts in that order of preference. PolyA tails were trimmed using

trimest (www.emboss.org), reduced to the most 3′ 500 bp using a custom script, and repeats were softmasked using RepeatMasker (www.repeatmasker.org). Arrayoligoselector (http://arrayoligosel.sourceforge.net) was used to design 65mer oligonucleotides with ~50% GC content that were unique in the genome when compared to all predicted transcripts from Zv4 (www.ensembl.org/Danio_rerio/index.html). Oligonucleotides with 5′ amino linkers were obtained from Illumina, spotted in duplicate and processed by the Sanger Microarray Facility on Codelink activated slides (GE Healthcare) according to the manufacturer's instructions. Each oligonucleotide probe is spotted twice on each array.

Approximately 600 Zebrafish embryos were collected from the London (Lon) strain in multiple clutches. Half of each clutch was injected with 4 ng of *ofd1*ATG MO and the other half with 4 ng of standard control MO (GeneTools) at 1-cell to 4-cell stage. Embryos were grown at 28°C until they reached the shield stage, when they were snap frozen on dry ice and stored at −80°C. Microarray analysis was performed as described in (73) with the following modifications. The Trizol extracted RNA samples were not purified by LiCl precipitation and 20 μg of each were used in direct reverse transcription labelling reactions using an oligo-dT18, 3 nmol of dCTP-Cy3 or dCTP-Cy5 (GE Heathcare) and Superscript II (Invitrogen). RNA was hydrolysed in 50 mM NaOH, neutralized in 50 mM HCl, cleaned with a QIAquick PCR Purification Kit column and paired labelled probes (control MO versus *ofd1* MO) were hybridized to microarray A-MEXP-1050 described in ArrayExpress (http://www.ebi.ac.uk/microarray-as/aer/details?templateName=Contact.vm&class=MAGE.ArrayDesign_designProviders&contextClass=MAGE.Contact&criteria=ArrayDesign%3D1582291058 in experiment E-MEXP-1879).

Slides were scanned at 10 μm resolution on a ScanArray HT (Perkin-Elmer) or 5 μm resolution on GenePix 4000B (Axon Instruments) and analysed using GenePix5.1. Data were Loess normalized (74) and analysed using the bioconductor (http://www.bioconductor.org/) limma package (75). Data were *P*-value adjusted (76) to yield a sorted list of differentially expression genes.

Real-time PCR

Total RNA was extracted from embryos at shield stage with Trizol and 500 ng were used for cDNA synthesis primed by random primers and performed with Superscript II RT (Invitrogen). Real-time PCR was performed using the Custom TaqMan® Gene Expression Assays purchased from Applied Biosystems. PCR reactions were carried out in an Applied Biosystems 7300 Real-Time PCR System machine. For calculations, the standard curve method was used (77). Genes selected as controls for normalization were *β-actin*, *ornithine decarboxylase 1* (*odc1*), *transcription elongation factor A* (*tcea1*) and *coatomer protein complex, subunit alpha* (*copa*). We repeated experiments three times using three different sets of embryos.

SUPPLEMENTARY MATERIAL

Supplementary Material is available at *HMG* Online.

ACKNOWLEDGEMENTS

We wish to thank Mark Turmaine for his help with the EM for glomeruli and Masatake Kai for useful advice on beads injection and tracking. We would also like to thank Sally Feather, Carla Lopes and Andrew Fry for discussions.

Conflict of Interest statement. None declared.

FUNDING

This work was supported by a Wellcome Trust grant to A.S.W. [075311], by Wellcome Trust Sanger Institute core support to D.L.S. [grant number WT077037/Z/05/Z] and by Wellcome Trust and BBSRC grants to S.W.W. Funding to pay the Open Access charge was provided by the Wellcome Trust [grant number WT077037/Z/05/Z].

REFERENCES

1. Gurrieri, F., Franco, B., Toriello, H. and Neri, G. (2007) Oral-facial-digital syndromes: review and diagnostic guidelines. *Am. J. Med. Genet. A*, **143**, 3314–3323.
2. Toriello, H.V. (1993) Oral-facial-digital syndromes, 1992. *Clin. Dysmorphol.*, **2**, 95–105.
3. Feather, S.A., Winyard, P.J., Dodd, S. and Woolf, A.S. (1997) Oral-facial-digital syndrome type 1 is another dominant polycystic kidney disease: clinical, radiological and histopathological features of a new kindred. *Nephrol. Dial. Transplant.*, **12**, 1354–1361.
4. Feather, S.A., Woolf, A.S., Donnai, D., Malcolm, S. and Winter, R.M. (1997) The oral-facial-digital syndrome type 1 (OFD1), a cause of polycystic kidney disease and associated malformations, maps to Xp22.2–Xp22.3. *Hum. Mol. Genet.*, **6**, 1163–1167.
5. Leao, M.J. and Ribeiro-Silva, M.L. (1995) Orofaciodigital syndrome type I in a patient with severe CNS defects. *Pediatr. Neurol.*, **13**, 247–251.
6. Romio, L., Wright, V., Price, K., Winyard, P.J., Donnai, D., Porteous, M.E., Franco, B., Giorgio, G., Malcolm, S., Woolf, A.S. *et al.* (2003) OFD1, the gene mutated in oral-facial-digital syndrome type 1, is expressed in the metanephros and in human embryonic renal mesenchymal cells. *J. Am. Soc. Nephrol.*, **14**, 680–689.
7. Romio, L., Fry, A.M., Winyard, P.J., Malcolm, S., Woolf, A.S. and Feather, S.A. (2004) OFD1 is a centrosomal/basal body protein expressed during mesenchymal-epithelial transition in human nephrogenesis. *J. Am. Soc. Nephrol.*, **15**, 2556–2568.
8. Giorgio, G., Alfieri, M., Prattichizzo, C., Zullo, A., Cairo, S. and Franco, B. (2007) Functional characterization of the OFD1 protein reveals a nuclear localization and physical interaction with subunits of a chromatin remodeling complex. *Mol. Biol. Cell.*, **18**, 4397–4404.
9. Ferrante, M.I., Giorgio, G., Feather, S.A., Bulfone, A., Wright, V., Ghiani, M., Selicorni, A., Gammaro, L., Scolari, F., Woolf, A.S. *et al.* (2001) Identification of the gene for oral-facial-digital type I syndrome. *Am. J. Hum. Genet.*, **68**, 569–576.
10. Thauvin-Robinet, C., Cossee, M., Cormier-Daire, V., Van Maldergem, L., Toutain, A., Alembik, Y., Bieth, E., Layet, V., Parent, P., David, A. *et al.* (2006) Clinical, molecular, and genotype-phenotype correlation studies from 25 cases of oral-facial-digital syndrome type 1: a French and Belgian collaborative study. *J. Med. Genet.*, **43**, 54–61.
11. Ferrante, M.I., Barra, A., Truong, J.P., Banfi, S., Disteche, C.M. and Franco, B. (2003) Characterization of the OFD1/Ofd1 genes on the human and mouse sex chromosomes and exclusion of Ofd1 for the Xpl mouse mutant. *Genomics*, **81**, 560–569.
12. Bisgrove, B.W. and Yost, H.J. (2006) The roles of cilia in developmental disorders and disease. *Development*, **133**, 4131–4143.
13. Sun, Z., Amsterdam, A., Pazour, G.J., Cole, D.G., Miller, M.S. and Hopkins, N. (2004) A genetic screen in zebrafish identifies cilia genes as a principal cause of cystic kidney. *Development*, **131**, 4085–4093.
14. Yoder, B.K., Tousson, A., Millican, L., Wu, J.H., Bugg, C.E. Jr, Schafer, J.A. and Balkovetz, D.F. (2002) Polaris, a protein disrupted in orpk mutant

mice, is required for assembly of renal cilium. *Am. J. Physiol. Renal. Physiol.*, **282**, F541–F552.
15. Nonaka, S., Tanaka, Y., Okada, Y., Takeda, S., Harada, A., Kanai, Y., Kido, M. and Hirokawa, N. (1998) Randomization of left-right asymmetry due to loss of nodal cilia generating leftward flow of extraembryonic fluid in mice lacking KIF3B motor protein. *Cell*, **95**, 829–837.
16. Essner, J.J., Amack, J.D., Nyholm, M.K., Harris, E.B. and Yost, H.J. (2005) Kupffer's vesicle is a ciliated organ of asymmetry in the zebrafish embryo that initiates left-right development of the brain, heart and gut. *Development*, **132**, 1247–1260.
17. Simons, M., Gloy, J., Ganner, A., Bullerkotte, A., Bashkurov, M., Kronig, C., Schermer, B., Benzing, T., Cabello, O.A., Jenny, A. *et al.* (2005) Inversin, the gene product mutated in nephronophthisis type II, functions as a molecular switch between Wnt signaling pathways. *Nat. Genet.*, **37**, 537–543.
18. Nauli, S.M., Alenghat, F.J., Luo, Y., Williams, E., Vassilev, P., Li, X., Elia, A.E., Lu, W., Brown, E.M., Quinn, S.J. *et al.* (2003) Polycystins 1 and 2 mediate mechanosensation in the primary cilium of kidney cells. *Nat. Genet.*, **33**, 129–137.
19. Fischer, E., Legue, E., Doyen, A., Nato, F., Nicolas, J.F., Torres, V., Yaniv, M. and Pontoglio, M. (2006) Defective planar cell polarity in polycystic kidney disease. *Nat. Genet.*, **38**, 21–23.
20. Corbit, K.C., Aanstad, P., Singla, V., Norman, A.R., Stainier, D.Y. and Reiter, J.F. (2005) Vertebrate Smoothened functions at the primary cilium. *Nature*, **437**, 1018–1021.
21. Haycraft, C.J., Banizs, B., Aydin-Son, Y., Zhang, Q., Michaud, E.J. and Yoder, B.K. (2005) Gli2 and Gli3 localize to cilia and require the intraflagellar transport protein polaris for processing and function. *PLoS Genet.*, **1**, e53.
22. Huangfu, D., Liu, A., Rakeman, A.S., Murcia, N.S., Niswander, L. and Anderson, K.V. (2003) Hedgehog signalling in the mouse requires intraflagellar transport proteins. *Nature*, **426**, 83–87.
23. Ferrante, M.I., Zullo, A., Barra, A., Bimonte, S., Messaddeq, N., Studer, M., Dolle, P. and Franco, B. (2006) Oral-facial-digital type I protein is required for primary cilia formation and left-right axis specification. *Nat. Genet.*, **38**, 112–117.
24. Corbit, K.C., Shyer, A.E., Dowdle, W.E., Gaulden, J., Singla, V. and Reiter, J.F. (2008) Kif3a constrains beta-catenin-dependent Wnt signalling through dual ciliary and non-ciliary mechanisms. *Nat. Cell Biol.*, **10**, 70–76.
25. Jones, C., Roper, V.C., Foucher, I., Qian, D., Banizs, B., Petit, C., Yoder, B.K. and Chen, P. (2008) Ciliary proteins link basal body polarization to planar cell polarity regulation. *Nat. Genet.*, **40**, 69–77.
26. Oishi, I., Kawakami, Y., Raya, A., Callol-Massot, C. and Izpisua Belmonte, J.C. (2006) Regulation of primary cilia formation and left-right patterning in zebrafish by a noncanonical Wnt signaling mediator, duboraya. *Nat. Genet.*, **38**, 1316–1322.
27. Park, T.J., Haigo, S.L. and Wallingford, J.B. (2006) Ciliogenesis defects in embryos lacking inturned or fuzzy function are associated with failure of planar cell polarity and Hedgehog signaling. *Nat. Genet.*, **38**, 303–311.
28. Jessen, J.R., Topczewski, J., Bingham, S., Sepich, D.S., Marlow, F., Chandrasekhar, A. and Solnica-Krezel, L. (2002) Zebrafish trilobite identifies new roles for Strabismus in gastrulation and neuronal movements. *Nat. Cell Biol.*, **4**, 610–615.
29. Tada, M. and Smith, J.C. (2000) Xwnt11 is a target of Xenopus Brachyury: regulation of gastrulation movements via Dishevelled, but not through the canonical Wnt pathway. *Development*, **127**, 2227–2238.
30. Heisenberg, C.P., Tada, M., Rauch, G.J., Saude, L., Concha, M.L., Geisler, R., Stemple, D.L., Smith, J.C. and Wilson, S.W. (2000) Silberblick/Wnt11 mediates convergent extension movements during zebrafish gastrulation. *Nature*, **405**, 76–81.
31. Keller, R. (2002) Shaping the vertebrate body plan by polarized embryonic cell movements. *Science*, **298**, 1950–1954.
32. Ross, A.J., May-Simera, H., Eichers, E.R., Kai, M., Hill, J., Jagger, D.J., Leitch, C.C., Chapple, J.P., Munro, P.M., Fisher, S. *et al.* (2005) Disruption of Bardet-Biedl syndrome ciliary proteins perturbs planar cell polarity in vertebrates. *Nat. Genet.*, **37**, 1135–1140.
33. Torban, E., Kor, C. and Gros, P. (2004) Van Gogh-like2 (Strabismus) and its role in planar cell polarity and convergent extension in vertebrates. *Trends Genet.*, **20**, 570–577.
34. Gerdes, J.M., Liu, Y., Zaghloul, N.A., Leitch, C.C., Lawson, S.S., Kato, M., Beachy, P.A., Beales, P.L., DeMartino, G.N., Fisher, S. *et al.* (2007) Disruption of the basal body compromises proteasomal function and perturbs intracellular Wnt response. *Nat. Genet.*, **39**, 1350–1360.
35. Badano, J.L., Mitsuma, N., Beales, P.L. and Katsanis, N. (2006) The ciliopathies: an emerging class of human genetic disorders. *Annu. Rev. Genomics Hum. Genet.*, **7**, 125–148.
36. Benzing, T., Simons, M. and Walz, G. (2007) Wnt signaling in polycystic kidney disease. *J. Am. Soc. Nephrol.*, **18**, 1389–1398.
37. Drummond, I. (2003) Making a zebrafish kidney: a tale of two tubes. *Trends Cell Biol.*, **13**, 357–365.
38. Anzenberger, U., Bit-Avragim, N., Rohr, S., Rudolph, F., Dehmel, B., Willnow, T.E. and Abdelilah-Seyfried, S. (2006) Elucidation of megalin/LRP2-dependent endocytic transport processes in the larval zebrafish pronephros. *J. Cell Sci.*, **119**, 2127–2137.
39. Hsu, H.J., Lin, G. and Chung, B.C. (2003) Parallel early development of zebrafish interrenal glands and pronephros: differential control by wt1 and ff1b. *Development*, **130**, 2107–2116.
40. Perner, B., Englert, C. and Bollig, F. (2007) The Wilms tumor genes wt1a and wt1b control different steps during formation of the zebrafish pronephros. *Dev. Biol.*, **309**, 87–96.
41. Yee, N.S., Yusuff, S. and Pack, M. (2001) Zebrafish pdx1 morphant displays defects in pancreas development and digestive organ chirality, and potentially identifies a multipotent pancreas progenitor cell. *Genesis*, **30**, 137–140.
42. Raya, A. and Belmonte, J.C. (2006) Left-right asymmetry in the vertebrate embryo: from early information to higher-level integration. *Nat. Rev. Genet.*, **7**, 283–293.
43. Long, S., Ahmad, N. and Rebagliati, M. (2003) The zebrafish nodal-related gene southpaw is required for visceral and diencephalic left-right asymmetry. *Development*, **130**, 2303–2316.
44. Liang, J.O., Etheridge, A., Hantsoo, L., Rubinstein, A.L., Nowak, S.J., Izpisua Belmonte, J.C. and Halpern, M.E. (2000) Asymmetric nodal signaling in the zebrafish diencephalon positions the pineal organ. *Development*, **127**, 5101–5112.
45. Bisgrove, B.W., Essner, J.J. and Yost, H.J. (1999) Regulation of midline development by antagonism of lefty and nodal signaling. *Development*, **126**, 3253–3262.
46. Goodrich, L.V., Johnson, R.L., Milenkovic, L., McMahon, J.A. and Scott, M.P. (1996) Conservation of the hedgehog/patched signaling pathway from flies to mice: induction of a mouse patched gene by Hedgehog. *Genes Dev.*, **10**, 301–312.
47. Ericson, J., Rashbass, P., Schedl, A., Brenner-Morton, S., Kawakami, A., van Heyningen, V., Jessell, T.M. and Briscoe, J. (1997) Pax6 controls progenitor cell identity and neuronal fate in response to graded Shh signaling. *Cell*, **90**, 169–180.
48. Barresi, M.J., Stickney, H.L. and Devoto, S.H. (2000) The zebrafish slow-muscle-omitted gene product is required for Hedgehog signal transduction and the development of slow muscle identity. *Development*, **127**, 2189–2199.
49. Concordet, J.P., Lewis, K.E., Moore, J.W., Goodrich, L.V., Johnson, R.L., Scott, M.P. and Ingham, P.W. (1996) Spatial regulation of a zebrafish patched homologue reflects the roles of sonic hedgehog and protein kinase A in neural tube and somite patterning. *Development*, **122**, 2835–2846.
50. Miyasaka, K.Y., Kida, Y.S., Sato, T., Minami, M. and Ogura, T. (2007) Csrp1 regulates dynamic cell movements of the mesendoderm and cardiac mesoderm through interactions with Dishevelled and Diversin. *Proc. Natl Acad. Sci. USA*, **104**, 11274–11279.
51. Moeller, H., Jenny, A., Schaeffer, H.J., Schwarz-Romond, T., Mlodzik, M., Hammerschmidt, M. and Birchmeier, W. (2006) Diversin regulates heart formation and gastrulation movements in development. *Proc. Natl Acad. Sci. USA*, **103**, 15900–15905.
52. Panizzi, J.R., Jessen, J.R., Drummond, I.A. and Solnica-Krezel, L. (2007) New functions for a vertebrate Rho guanine nucleotide exchange factor in ciliated epithelia. *Development*, **134**, 921–931.
53. Sarrazin, A.F., Villablanca, E.J., Nunez, V.A., Sandoval, P.C., Ghysen, A. and Allende, M.L. (2006) Proneural gene requirement for hair cell differentiation in the zebrafish lateral line. *Dev. Biol.*, **295**, 534–545.
54. Obara, T., Mangos, S., Liu, Y., Zhao, J., Wiessner, S., Kramer-Zucker, A.G., Olale, F., Schier, A.F. and Drummond, I.A. (2006) Polycystin-2 immunolocalization and function in zebrafish. *J. Am. Soc. Nephrol.*, **17**, 2706–2718.
55. Otto, E.A., Schermer, B., Obara, T., O'Toole, J.F., Hiller, K.S., Mueller, A.M., Ruf, R.G., Hoefele, J., Beekmann, F., Landau, D. *et al.* (2003) Mutations in INVS encoding inversin cause nephronophthisis type 2,

linking renal cystic disease to the function of primary cilia and left-right axis determination. *Nat. Genet.*, **34**, 413–420.
56. McGrath, J., Somlo, S., Makova, S., Tian, X. and Brueckner, M. (2003) Two populations of node monocilia initiate left-right asymmetry in the mouse. *Cell*, **114**, 61–73.
57. Kreiling, J.A., Williams, G. and Creton, R. (2007) Analysis of Kupffer's vesicle in zebrafish embryos using a cave automated virtual environment. *Dev. Dyn.*, **236**, 1963–1969.
58. Kramer-Zucker, A.G., Olale, F., Haycraft, C.J., Yoder, B.K., Schier, A.F. and Drummond, I.A. (2005) Cilia-driven fluid flow in the zebrafish pronephros, brain and Kupffer's vesicle is required for normal organogenesis. *Development*, **132**, 1907–1921.
59. Slater, G.S. and Birney, E. (2005) Automated generation of heuristics for biological sequence comparison. *BMC Bioinformatics*, **6**, 31.
60. Li, H., Coghlan, A., Ruan, J., Coin, L.J., Heriche, J.K., Osmotherly, L., Li, R., Liu, T., Zhang, Z., Bolund, L. *et al.* (2006) TreeFam: a curated database of phylogenetic trees of animal gene families. *Nucleic Acids Res.*, **34**, D572–D580.
61. Budny, B., Chen, W., Omran, H., Fliegauf, M., Tzschach, A., Wisniewska, M., Jensen, L.R., Raynaud, M., Shoichet, S.A., Badura, M. *et al.* (2006) A novel X-linked recessive mental retardation syndrome comprising macrocephaly and ciliary dysfunction is allelic to oral-facial-digital type I syndrome. *Hum. Genet.*, **120**, 171–178.
62. Ibanez-Tallon, I., Pagenstecher, A., Fliegauf, M., Olbrich, H., Kispert, A., Ketelsen, U.P., North, A., Heintz, N. and Omran, H. (2004) Dysfunction of axonemal dynein heavy chain Mdnah5 inhibits ependymal flow and reveals a novel mechanism for hydrocephalus formation. *Hum. Mol. Genet.*, **13**, 2133–2141.
63. Banizs, B., Komlosi, P., Bevensee, M.O., Schwiebert, E.M., Bell, P.D. and Yoder, B.K. (2007) Altered pH(i) regulation and Na(+)/HCO3(−) transporter activity in choroid plexus of cilia-defective Tg737(orpk) mutant mouse. *Am. J. Physiol. Cell Physiol.*, **292**, C1409–C1416.
64. Lechtreck, K.F., Delmotte, P., Robinson, M.L., Sanderson, M.J. and Witman, G.B. (2008) Mutations in Hydin impair ciliary motility in mice. *J. Cell Biol.*, **180**, 633–643.
65. Lowery, L.A. and Sive, H. (2005) Initial formation of zebrafish brain ventricles occurs independently of circulation and requires the nagie oko and snakehead/atp1a1a.1 gene products. *Development*, **132**, 2057–2067.
66. Tsujikawa, M. and Malicki, J. (2004) Intraflagellar transport genes are essential for differentiation and survival of vertebrate sensory neurons. *Neuron*, **42**, 703–716.
67. Prattichizzo, C., Macca, M., Novelli, V., Giorgio, G., Barra, A. and Franco, B. (2008) Mutational spectrum of the oral-facial-digital type I syndrome: a study on a large collection of patients. *Hum. Mutat.*, **29**, 1237–1246.
68. Kishimoto, N., Cao, Y., Park, A. and Sun, Z. (2008) Cystic kidney gene seahorse regulates cilia-mediated processes and Wnt pathways. *Dev. Cell*, **14**, 954–961.
69. Majumdar, A. and Drummond, I.A. (2000) The zebrafish floating head mutant demonstrates podocytes play an important role in directing glomerular differentiation. *Dev. Biol.*, **222**, 147–157.
70. Beckers, A., Alten, L., Viebahn, C., Andre, P. and Gossler, A. (2007) The mouse homeobox gene Noto regulates node morphogenesis, notochordal ciliogenesis, and left right patterning. *Proc. Natl Acad. Sci. USA*, **104**, 15765–15770.
71. Kimmel, C.B., Ballard, W.W., Kimmel, S.R., Ullmann, B. and Schilling, T.F. (1995) Stages of embryonic development of the zebrafish. *Dev. Dyn.*, **203**, 253–310.
72. Thisse, C. and Thisse, B. (2008) High-resolution in situ hybridization to whole-mount zebrafish embryos. *Nat. Protoc.*, **3**, 59–69.
73. Goda, T., Abu-Daya, A., Carruthers, S., Clark, M.D., Stemple, D.L. and Zimmerman, L.B. (2006) Genetic screens for mutations affecting development of Xenopus tropicalis. *PLoS Genet.*, **2**, e91.
74. Yang, Y.H., Dudoit, S., Luu, P., Lin, D.M., Peng, V., Ngai, J. and Speed, T.P. (2002) Normalization for cDNA microarray data: a robust composite method addressing single and multiple slide systematic variation. *Nucleic Acids Res.*, **30**, e15.
75. Smyth, G.K. (2004) Linear models and empirical bayes methods for assessing differential expression in microarray experiments. *Stat. Appl. Genet. Mol. Biol.*, **3**, http://www.bepress.com/sagmb/vol3/iss1/art3.
76. Benjamini, Y. and Hochberg, Y. (1995) Controlling the false discovery rate: a practical and powerful approach to multiple testing. *J. Roy. Stat. Soc., Ser. B*, **57**, 289–300.
77. Rajeevan, M.S., Ranamukhaarachchi, D.G., Vernon, S.D. and Unger, E.R. (2001) Use of real-time quantitative PCR to validate the results of cDNA array and differential display PCR technologies. *Methods*, **25**, 443–451.